Correlation of CRM1-NES affinity with nuclear export activity

Szu-Chin Fu, Ho Yee Joyce Fung, Tolga Cağatay, Jordan Baumhardt, and Yuh Min Chook*
Department of Pharmacology, University of Texas Southwestern Medical Center, Dallas, TX 75390

ABSTRACT CRM1 (Exportin1/XPO1) exports hundreds of broadly functioning protein cargoes out of the cell nucleus by binding to their classical nuclear export signals (NESs). The 8- to 15-amino-acid-long NESs contain four to five hydrophobic residues and are highly diverse in both sequence and CRM1-bound structure. Here we examine the relationship between nuclear export activities of 24 different NES peptides in cells and their CRM1-NES affinities. We found that binding affinity and nuclear export activity are linearly correlated for NESs with dissociation constants (K_ds) between tens of nanomolar to tens of micromolar. NESs with K_ds outside this range have significantly reduced nuclear export activities. These include two unusually tight-binding peptides, one from the nonstructural protein 2 of murine minute virus (MVM NS2) and the other a mutant of the protein kinase A inhibitor (PKI) NES. The crystal structure of CRM1-bound MVM NS2[NES] suggests that extraordinarily tight CRM1 binding arises from intramolecular contacts within the NES that likely stabilizes the CRM1-bound conformation in free peptides. This mechanistic understanding led to the design of two novel peptide inhibitors that bind CRM1 with picomolar affinity.

INTRODUCTION

Nuclear-cytoplasmic transport of macromolecules is largely mediated by karyopherin-β family nuclear transport receptors (Kaps; importins and exportins). Importins bind their cargoes in the cytoplasm and release them in the nucleus whereas exportins mediate the reverse process. The chromosome region maintenance 1 (CRM1) protein (also known as exportin-1 or XPO1) binds 8- to 15-residues-long nuclear export signals (NESs) in hundreds of different protein cargoes (Fornerod *et al.*, 1997; Fukuda *et al.*, 1997; Ossareh-Nazari *et al.*, 1997; Stade *et al.*, 1997; Thakar *et al.*, 2013). The repertoire of the protein cargoes of CRM1 continues to grow; ~250 experimentally identified protein cargoes are recorded in NES databases Valid-NESs and NESdb (Fu *et al.*, 2012; Xu *et al.*, 2012, 2015), and over 1000 putative CRM1 cargoes were identified in a recent proteomics study (Kırlı *et al.*, 2015). Accordingly, the diversity of NES sequences has also grown with ever-expanding NES patterns that result in many false positives when used in NES prediction. Further complexity is observed as recent structural analysis of 13 different CRM1-NES complexes revealed a large range of NES backbone conformations (Fung *et al.*, 2017). Nevertheless, the study of NES recognition by CRM1 is important as CRM1-NES interactions are the targets of small molecule inhibitors such as Selinexor/KPT-330, Eltanexor/KPT-8602, Verdinexor/KPT-335, KPT-350 (Karyopharm), and SL801 (Stemline), which are being tested in clinical trials for a variety of cancers and inflammatory diseases or as an antiviral agent.

In addition to CRM1, the importin α/β (Impα/β) system also recognizes hundreds to thousands of broadly functioning cargoes, in this case proteins that contain the classical nuclear localization signal (cNLS). Extensive structural, biochemical, and cell biological studies of cNLS recognition by Impα preceded analogous CRM1-NES studies (Conti *et al.*, 1998; Kobe, 1999; Marfori *et al.*, 2011). More than 80 crystal structures of Impα-cNLS complexes are available, showing how various poly-basic monopartite and bipartite cNLS peptides interact with two binding sites on several Impα isoforms. Nuclear import activities of different cNLS peptides in cells and their affinities for Impα were measured and compared (Fanara *et al.*, 2000; Hodel *et al.*, 2001, 2006). These studies roughly divided cNLSs into three groups: 1) active NLSs with K_Ds from 1 nM to hundreds of nanomolar where nuclear import appears to correlate with Impα-cNLS affinity, 2) inactive NLSs with dissociation constants (K_Ds) in the

micromolar range, and 3) NLSs that bind with K_ds < 1 nM, which exhibited a saturated maximum nuclear import activity (Hodel *et al.*, 2006). More recent studies have shown two nonclassical nuclear localization signal (ncNLS) that bind exclusively to the minor NLS-binding site of importin-α with micromolar affinities are also active NLSs in cells. These studies suggest that binding affinities between active NLSs and Impα can vary over three orders of magnitude with K_ds ranging from nanomolar to micromolar (Lott *et al.*, 2011; Nakada *et al.*, 2015; Wu *et al.*, 2017). However, no equivalent studies of the dynamic range of nuclear export activity versus CRM1-NES affinity have been reported.

Here we measured the cytoplasmic-to-nuclear ratios, in live cells, of a fluorescent reporter that is fused to 24 different NES sequences to report on nuclear export activities of the NESs. Comparison with their affinities for CRM1 revealed a strong linear correlation of nuclear export activity and CRM1-NES affinity for NESs that bind CRM1 with K_ds that range from tens of nanomolar to tens of micromolar. Peptides that bind CRM1 with K_ds > 150 μM do not direct nuclear export in cells, suggesting an upper limit in CRM1-NES K_d values for optimal nuclear export. When NESs bind CRM1 with K_ds < 5 nM, their nuclear export activities are also significantly reduced. These supertight NESs also inhibit nuclear export of average NESs. Structure of a supertight peptide bound to CRM1 showed intramolecular contacts that were not observed in other CRM1-NES structures. The use of this unusual NES structural element led to the design of two peptide inhibitors that bind CRM1 with picomolar affinity.

RESULTS AND DISCUSSION
Measuring NES activity in live cells
We selected 24 different NES peptides to measure nuclear export activities in cells. The NESs were selected to sample a broad range of affinity for CRM1 based on qualitative estimates from previous pull-down binding assays (Xu *et al.*, 2012, 2015). The NES from protein kinase A inhibitor (PKI[NES]; [34]NSNELALKLAGLDINK[49]) was used as positive control. Two known inactive PKI[NES] mutants, PKI[NES](I47A) and PKI[NES](L42A/L45A), served as negative controls (Wen *et al.*, 1995). Plasmids encoding enhanced yellow fluorescent protein (EYFP$_2$)-SV40[NLS]-NES fusion proteins were transfected into HeLa cells and the nuclear-cytoplasmic distribution of the fluorescent reporter proteins were recorded by live cell confocal microscopy. The ratio of mean fluorescence intensity of EYFP$_2$-SV40[NLS]-NES in the cytoplasm to mean fluorescence intensity in the nucleus ($R_{C/N}$) is used as a measure of nuclear export activity. CRM1-mediated nuclear export was demonstrated by nuclear accumulation of EYFP$_2$-SV40[NLS]-NES following treatment with 5 nM leptomycin B (LMB) for 16–18 h. Since LMB inhibits CRM1, the $R_{C/N}$ with LMB treatment can account for passive export of reporter proteins by diffusion. Therefore, we normalized observed $R_{C/N}$ of each NES peptide with its corresponding $R_{C/N}$ value on LMB treatment. The quantitative workflow of the imaging study is described in Figure 1A. Representative images of inactive, moderate and strong NESs are shown in Figure 1B (all other NESs are shown in Supplemental Figure S1A).

To examine the impact of variation in reporter protein expression on nuclear export activity among different cells, we analyzed the correlation between $R_{C/N}$ and the expression level of EYFP$_2$-SV40[NLS]-NES in the cell. As shown in Supplemental Figure S2A, $R_{C/N}$ values are plotted for individual HeLa cells as a function of the mean fluorescence intensity of the whole cell. Analysis of four different NESs (EYFP$_2$-SV40[NLS]-Stradα[NES], EYFP$_2$-SV40[NLS]-HIV Rev[NES], EYFP$_2$-SV40[NLS]-MEK1[NES], and EYFP$_2$-SV40[NLS]-MVM NS2[NES]) showed no correlation between the $R_{C/N}$ and the expression level of reporter proteins in the cell, suggesting that variation in expression level (at least across the range examined here) does not affect CRM1-mediated export of the reporter proteins.

Measuring CRM1-NES affinities
CRM1-NES binding affinities (dissociation constants or K_ds) were measured using a previously described differential bleaching assay, with purified CRM1 and NES proteins in the presence of excess RanGTP (Fung *et al.*, 2015). MBP-NES fusion proteins were used as the MBP tag does not affect interactions with CRM1 (Fung *et al.*, 2015). K_d values are reported with 95% confidence intervals obtained using error-surface projection method. The K_d values of the 24 different NESs binding to CRM1 range from low nanomolar to a hundred micromolar (Table 1; differential bleaching data shown in Supplemental Figure S3, A and B). Negative controls, PKI[NES](I47A) and PKI[NES](L42A/L45A) mutants (Wen *et al.*, 1995), have K_d values >150 μM, suggesting extremely weak binding. Analysis of simulated differential bleaching data in PALMIST (Scheuermann *et al.*, 2016) indicated that the high-affinity detection limit of our experiments is ~1 nM K_d (Supplemental Figure S3C; see details under *Materials and Methods*). Therefore, K_d values of several high-affinity NESs (Super PKI[NES] and MVM NS2[NES]; Table 1) are beyond the limit of accurate determination. K_ds with undefined confidence intervals are reported as such and are used for rough comparisons.

Comparing NES activities in cells and CRM1-NES affinities
We plotted CRM1-NES affinity ($\log_{10}K_d$, where K_d is in nanomolar) as a function of its $R_{C/N}$ or nuclear export activity. Both parameters are presented with error bars showing their respective 95% confidence limits (Figure 1C). The plot revealed a strong negative correlation between $\log_{10}K_d$ and $R_{C/N}$ as indicated by Pearson's $r = –0.65$ ($p = 0.0006$). Active NESs have an impressively wide range of affinities for CRM1 that span four orders of magnitude, from K_ds of single-digit nanomolar to tens of micromolar. The NES from the murine minute virus nonstructural protein 2 (MVM NS2[NES]) has the highest affinity for CRM1 ($K_d = 2$ nM). At the other end, there are four active NESs with K_ds of tens of micromolar: Stradα[NES] ($K_d = 10$ μM), SNUPN[NES] ($K_d = 13$ μM), CDC7[NES] ($K_d = 20$ μM), and HPV E7[NES] ($K_d = 34$ μM). The measured K_ds of two known inactive PKI[NES] mutants are 150 and 900 μM, respectively. Interestingly, two unusually tight-binding NES peptides with K_ds < 5 nM also have low nuclear export activity in cells. One of the supertight NES is MVM NS2[NES], while the other is the N35L mutant of PKI[NES], termed the Super PKI[NES], which was previously designed to increase CRM1 affinity for crystallographic study (Güttler *et al.*, 2010). When these two unusually tight-binding NESs were excluded from the analysis, the correlation coefficient between CRM1 affinity and nuclear export activity increased to a Pearson's $r = –0.87$ ($p = 1.48 \times 10^{-7}$). We note that interactions between CRM1 and full-length cargo proteins may be more complicated and require further investigations that include physiological concentrations of CRM1, cargoes, Ran, and other cargo proteins. Caution is advised when translating the K_ds reported in this study into CRM1-full-length cargo affinities.

It is generally thought that karyopherin-NLS/NES interactions should occur within a range of affinity suitable for both binding in one cell compartment and release in the other compartment. The two inactive PKI[NES] mutants PKI[NES](I47A) and PKI[NES](L42A/L45A) (Wen *et al.*, 1995) have $R_{C/N}$ values of 0.03 and 0.01 that are consistent with their lack of activity (Table 1). The measured K_d of PKI[NES](I47A) for CRM1 is 150 [90, 310] μM (values in bracket represent 95% confidence interval). The next weakest CRM1 binder is the HPV E7[NES] ($K_d = 34$ [22, 53] μM), which has a significantly higher $R_{C/N}$

A

Living HeLa cells transfected with YFP$_2$-NLS-NES fusion proteins and stained with Hoechst

↓

Select cells that express fusion proteins and contain no obvious abnormality observed under DIC

↓

Search the middle focal-plane of nuclei via Hoechst

↓

Acquire a z–stack of images at the YFP and Hoechst channels

↓

Acquire a single DIC image

↓

Collapse selected z-stacks into a single image using ImageJ/Fiji

↓

Identify the nuclear region based on Hoechst stain

↓

Segment whole cell using DIC image, dilate nucleus mask and create a cytoplasmic ring

↓

Calculate the ratio of cytoplasmic/nuclear fluorescence intensity (C/N ratio) after background subtraction

↓

Normalize C/N ratio by LMB-treated cells

↓

Present nuclear export activity as the mean C/N ratio and 95% confidence intervals

Repeat for a minimum of 30 representative cells from 3 independent experiments

C

Binding Affinity vs. Nuclear Export Activity

Legend: PKI, CPEB4, MEK1, ADAR1, FMRP, hRio2, Super PKI, NPM^{mutA}, X11L2, mDia2, Pax, CPRB4-R, HIV Rev, p73, HDAC5, SMAD4, MVM NS2, hRio2-R, HPV E7, CDC7, Stradα, SNUPN, PKI^{I47A}, PKI$^{L42A/L45A}$

$K_D = 150\text{uM}$, $K_D = 34\text{uM}$, $K_D = 34\text{nM}$, $K_D = 2\text{nM}$

Pearson's r = -0.65; p = 0.0006

y-axis: $\log_{10} K_D$ (K_D in nanomolar)
x-axis: $R_{C/N}$

B

EYFP$_2$-SV40^{NLS}-PKI^{NES} EYFP$_2$-SV40^{NLS}-HIV Rev^{NES} EYFP$_2$-SV40^{NLS}-CDC7^{NES}
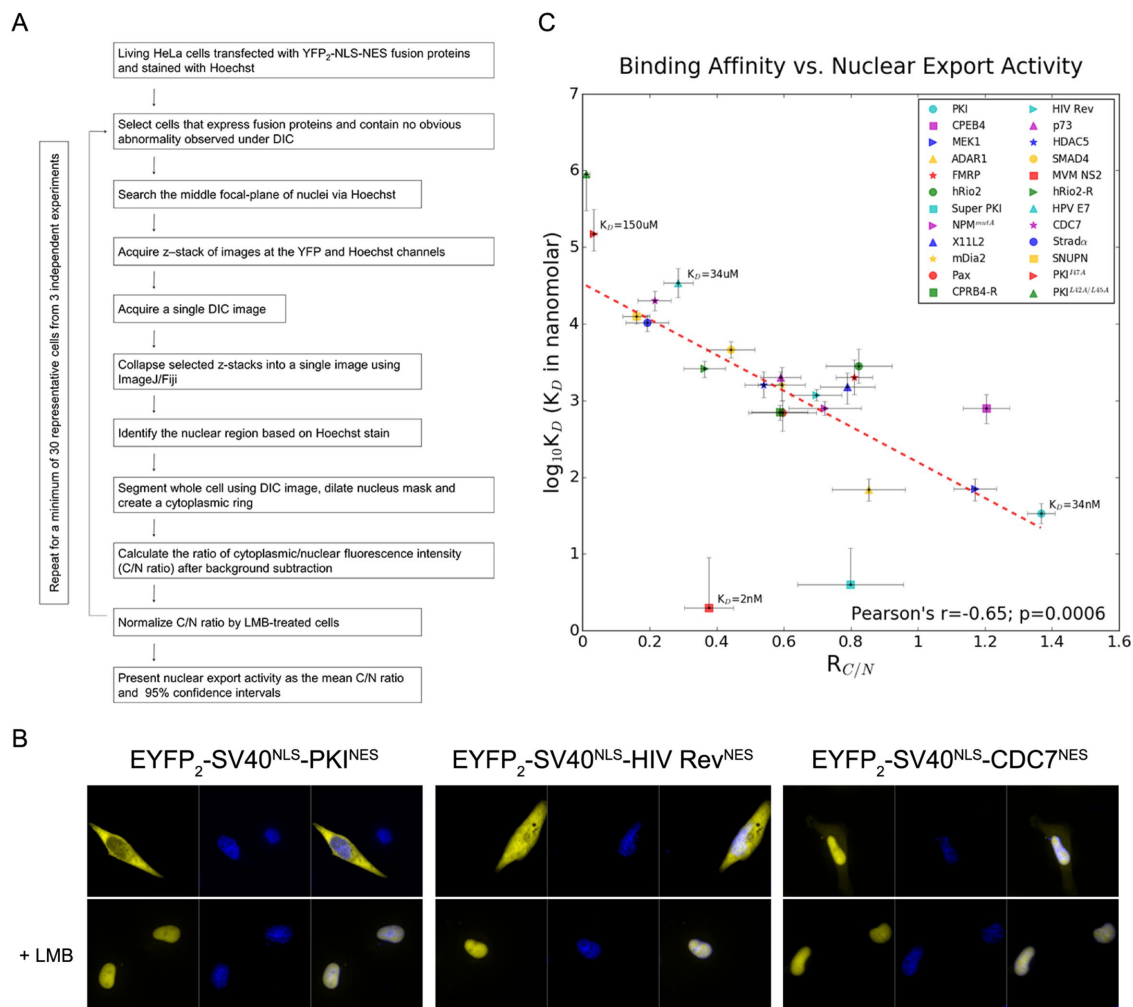
+ LMB

FIGURE 1: Correlation of NES export activity with binding affinity to CRM1. (A) Schematic of the workflow to quantify the ratio of cytoplasmic to nuclear mean fluorescence intensity ($R_{C/N}$). $R_{C/N}$ values are used as a measurement of NES activity in living HeLa cells. The loop in the workflow indicates that this process is repeated for at least 30 representative cells collected from at least three independent experiments (listed in Table 2) for statistical analysis. (B) Leptomycin B (LMB) sensitive nuclear export activity of EYFP$_2$-SV40^{NLS}-NES fusion proteins in HeLa cells. YFP (pseudocolored in yellow) and Hoechst (pseudocolored in blue) images were captured using spinning disk confocal microscope (40×). From left to right, PKI^{NES}, HIV Rev^{NES}, and CDC7^{NES}. Nuclear accumulation after treatment with 5 nM leptomycin B (+LMB) for 16–18 h demonstrates CRM1-dependent export. Representative images of all other NESs are shown in Supplemental Figure S1A. (C) Correlation of in vitro affinity and in vivo nuclear export activity. In vitro binding affinities of 24 NESs (includes two negative controls PKI^{NES}(I47A) and PKI^{NES}(L42A/L45A)) are plotted as a function of their nuclear export activities. Error bars represent 95% confidence intervals. Half of the vertical error bars for the binding affinities of PKI^{NES}(L42A/L45A), Super PKI^{NES}, and MVM NS2^{NES} are missing because the upper or lower limits are undetermined. The Pearson's r value of the 24 NESs is –0.65 ($p = 0.0006$) and is –0.87 ($p = 1.48 \times 10^{-7}$) when Super PKI^{NES} and MVM NS2^{NES} are not included.

value of 0.29. On the basis of these data points, we suggest that the lower limit of binding affinity for active nuclear export likely lie between 34 and 150 µM.

CRM1-NES interactions must also occur at affinities suitable for cargo/NES release in the cytoplasm. Therefore, there is likely an upper limit of CRM1-NES affinity for optimal nuclear export. An NES or cargo that binds CRM1 tighter than this limit will likely remain bound to CRM1 after RanGTP is hydrolyzed to RanGDP in the cytoplasm and potentially be taken back into the nucleus. Two NESs that bind CRM1 with K_ds < 5 nM, Super PKI^{NES} (K_d = 4 [U, 12] nM; U cannot be defined) and MVM NS2^{NES} (K_d = 2 [U, 9] nM), exhibit 42–72% lower nuclear export activity than the lower affinity PKI^{NES} (K_d = 34 [25, 46] nM). These results suggest that the upper limit of CRM1-NES affinity

for optimal nuclear export activity lies between 4 and 34 nM. Previous studies (Engelsma *et al.*, 2008; Güttler *et al.*, 2010) and pull-down binding data shown in Supplemental Figure S3D show that these two unusually tight-binding NESs can bind CRM1 in the absence of RanGTP, suggesting that their interactions with CRM1 in cells may be independent of Ran.

The supertight NESs can inhibit nuclear export

A protein or peptide that binds CRM1 too tightly may outcompete bona fide cargoes. Engineered peptides like the Bimax or M9M peptides, which bind Impα or Kapβ2, respectively, with picomolar affinities, are inhibitors of the karyopherins (Cansizoglu *et al.*, 2007; Kosugi *et al.*, 2008). We wondered whether the

NES	Mean $R_{C/N}$	$R_{C/N}$ 95% confidence interval		K_d (nM)	K_d 95% confidence interval	
		Low	High		Low	High
PKI	1.37	1.33	1.41	34[b]	25	46
CPEB4	1.20	1.13	1.27	800[b]	500	1200
MEK1[a]	1.17	1.11	1.23	70	40	130
ADAR1[a]	0.85	0.75	0.96	69	49	96
hRio2	0.82	0.72	0.92	2800[b]	1700	4700
FMRP	0.81	0.76	0.86	2000	1200	3400
Super PKI[a]	0.80	0.64	0.96	4	U[c]	12
X11L2	0.79	0.71	0.87	1500	900	2300
NPM[mutA]	0.72	0.61	0.83	790	640	980
HIV Rev[a]	0.70	0.62	0.77	1180	990	1400
Pax	0.60	0.49	0.70	700	400	1000
mDia2	0.59	0.52	0.66	1600	1000	2700
CPEB4-R	0.59	0.50	0.67	710[b]	560	880
p73[a]	0.59	0.53	0.65	2000	1700	2400
HDAC5	0.54	0.48	0.60	1600	1100	2400
SMAD4	0.44	0.37	0.51	4600	3600	5900
MVM NS2[a]	0.38	0.30	0.45	2	U[c]	9
hRio2-R	0.36	0.30	0.43	2600[b]	2000	3300
HPV E7[a]	0.29	0.24	0.33	34,000	22,000	53,000
CDC7	0.21	0.16	0.26	20,000	15,000	27,000
Stradα[a]	0.19	0.13	0.26	10,300	8000	13,000
SNUPN	0.16	0.12	0.20	12,500[b]	10,000	15,000
PKI (I47A)	0.03	0.02	0.04	150,000	90,000	310,000
PKI (L42A/L45A)[a]	0.01	0.00	0.02	900,000	300,000	U[c]

[a]Binding affinities measured in this study. Others were measured in our previous studies and reanalyzed to obtain 95% confidence interval.

[b]K_d reported here are slightly different from before as all data are now fitted using averages of triplicate experiments without weighted fitting. The absolute numbers are only slightly different from previously reported and differences are insignificant.

[c]U, cannot be defined.

TABLE 1: In vitro CRM1 binding affinity and in vivo activity of NESs.

unusually tight Super PKI[NES] and MVM NS2[NES] can function as CRM1 inhibitors. We cotransfected HeLa cells with EYFP$_2$-SV40[NLS]-PKI[NES] and either RFP-MVM NS2[NES] or RFP-Super PKI[NES]. Figure 2A shows that transfection with either RFP-MVM NS2[NES] or RFP-Super PKI[NES] decreased nuclear export of PKI[NES] substantially (by 74–87%). The inhibitory effect here is similar to but not as strong as that of leptomycin B (LMB), a very potent small molecule covalent inhibitor of CRM1, which decreased nuclear export of PKI[NES] by 92%. Interestingly, cotransfection of a strong NES like RFP-PKI[NES] (K_d = 34 nM) with EYFP$_2$-SV40[NLS]-X11L2[NES] did not affect nuclear export of weaker-binding X11L2[NES] (K_d = 1500 nM; Figure 2B). These results suggest that only the extraordinarily tight-binding NESs, with K_ds below the active NES limit, can indeed inhibit nuclear export of other NESs. Representative images of cells cotransfected with reporter proteins (EYFP$_2$-SV40[NLS]-PKI[NES]) and RFP-tagged competitive peptides, or treated with LMB, are shown in Figure 2C. In addition, the mean RFP and YFP intensities of the whole cell were measured and used to calculate the expression ratio of competitive peptide to reporter in individual cells (Supplemental Figure S1C).

Crystal structure of MVM NS2$_{NES}$ bound to CRM1

The structure of Super PKI[NES] (fused to the Snurportin-1 protein) bound to CRM1 showed the leucine in the N35L mutation site binding in the P0 pocket of the CRM1 NES-binding groove. This additional contact increases the number of anchoring hydrophobic residues from four in wild-type PKI[NES] to five in the supertight mutant (Güttler et al., 2010). It is unclear from the sequence of MVM NS2[NES] ([77]STVDEMTKKFGTLTIHD[93]) why it binds CRM1 so tightly. Using the engineered CRM1-Ran-RanBP1-NES quaternary complex (Fung et al., 2015), we solved the 2.0-Å resolution crystal structure of MVM NS2[NES] bound to CRM1 (Figure 3A, crystallographic statistics in Supplemental Table S1, and electron densities for the NES peptide in Figure 3B). MVM NS2[NES] binds CRM1 with the common NES conformation of an N-terminal α-helix followed by a C-terminal strand. Five hydrophobic side chains of MVM NS2[NES] (Val79, Met82, Phe86, Leu89, and Leu91) occupy the five hydrophobic pockets in the CRM1 groove (Figure 3A, left panel). The structures of CRM1-bound Super PKI[NES] and MVM NS2[NES] are highly similar (Cα root mean square deviation [r.m.s.d.] of 0.7 Å for 13 NES residues) and the NES-bound CRM1 grooves are virtually identical (Cα r.m.s.d. of
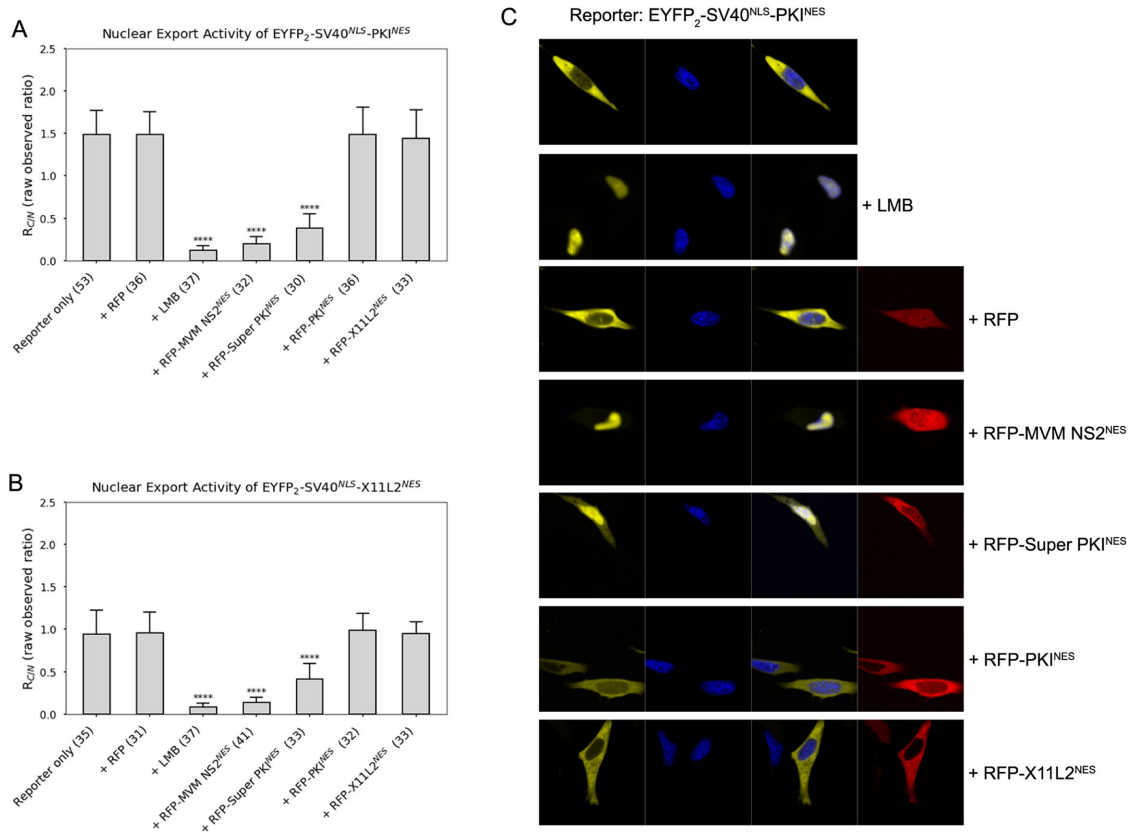
FIGURE 2: Inhibitory effect of extraordinary tight-binding NESs. (A) EYFP$_2$-SV40^{NLS}-PKI^{NES} is cotransfected with RFP, RFP-MVM NS2^{NES}, RFP-Super PKI^{NES}, RFP-PKI^{NES}, or RFP- X11L2^{NES} and compared with cells expressing EYFP$_2$-SV40^{NLS}-PKI^{NES} that are treated with small molecule inhibitor LMB. (B) EYFP$_2$-SV40^{NLS}-X11L2^{NES} is cotransfected with RFP, RFP-MVM NS2^{NES}, RFP-Super PKI^{NES}, RFP-PKI^{NES}, or RFP-X11L2^{NES} and compared with cells expressing EYFP$_2$-SV40^{NLS}-PKI^{NES} that are treated with small molecule inhibitor LMB. The numbers of examined cells from at least three independent experiments are indicated in parentheses in A and B. Error bars represent SD. The p values were calculated in comparison to control (reporter only) using Mann–Whitney tests. Note that observed $R_{C/N}$ values are presented without normalization to compare with $R_{C/N}$ on LMB treatment (+LMB). (C) Representative images of cells transfected with EYFP$_2$-SV40^{NLS}-PKI^{NES} (reporter) and RFP-tagged NESs (competitive peptides). YFP (pseudocolored in yellow), Hoechst (pseudocolored in blue), and RFP (pseudocolored in red) images were captured using spinning disk confocal microscope (40×). The expression levels of reporter proteins and competitive peptides and are summarized in Supplemental Figure S1C.

0.5 Å for 85 CRM1 groove residues). However, unique to CRM1-bound MVM NS2^{NES} are two intramolecular polar contacts involving the C-terminal strand of MVM NS2^{NES} (Figure 3A, right panel). Thr90 of MVM NS2^{NES} makes hydrogen bonds with both the side chain and main chain amides of MVM NS2^{NES} His92. These intrapeptide contacts likely stabilize the configuration of the C-terminal strand, perhaps preorganizing the structural element, for the unusual high-affinity binding to CRM1. Such intramolecular NES contacts have not been observed in any other CRM1-NES structures (Dong et al., 2009; Güttler et al., 2010; Fung et al., 2015, 2017).

Structure-based design of novel peptide inhibitors

To investigate the importance of the unusual intrapeptide contacts seen in CRM1-bound MVM NS2^{NES}, we generated chimeric NES peptides where ^{89}LTIHD^{93} of MVM NS2^{NES} is fused to N-terminal helical portions of other NESs. We asked whether the ^{89}LTIHD^9 strand of MVM NS2^{NES}, which contains the intramolecular contacts, could increase affinities of the chimeric NES peptides for CRM1. Fusion of ^{89}LTIHD^{93} to the very tight-binding Super PKI^{NES} (K_d = 4 [U, 12] nM) resulted in chimeric mutant Super PKI-NS2^{NES}

(NLELALKAGLTIHD). Fusion to the weak-binding CDC7^{NES} (K_d = 20 [15, 27] µM) gave chimera CDC7-NS2^{NES} (QDLRKLCERLRGLTIHD) (Figure 3C). Differential bleaching measurement of MBP-Super PKI-NS2^{NES} and MBP-CDC7-NS2^{NES} binding to CRM1 gave K_d values of 7 [U,U] and 27 [U,U] pM, respectively. Both chimeric peptides have picomolar affinity beyond the limit of accurate determination with our method (Figure 3D). These results indicate that the C-terminal ^{89}LTIHD^{93} residues of MVM NS2^{NES} contribute significant binding energy for interactions with CRM1. The transfer of this MVM NS2^{NES} segment can increase affinities of other NESs by as much as 4 orders of magnitude (K_d of CDC7-NS2^{NES} ≪ 1 nM vs. K_d of CDC7^{NES} = 20 µM). More importantly, the intramolecular contacts within ^{89}LTIHD^{93} appear to contribute significantly to the increased affinity of the NESs. The differences between Super PKI^{NES} and Super PKI-NS2^{NES} occur only in non-Φ residues; LDINK in Super PKI^{NES} vs. LTIHD in Super PKI-NS2^{NES} (Φ residues in bold; Figure 3C). The three-residue change increased binding affinity from 4 nM to ≪ 1 nM. We show that the picomolar affinity Super PKI-NS2^{NES} peptide is an effective CRM1 inhibitor in the cell (Supplemental Figure S1B), much like the engineered M9M peptide
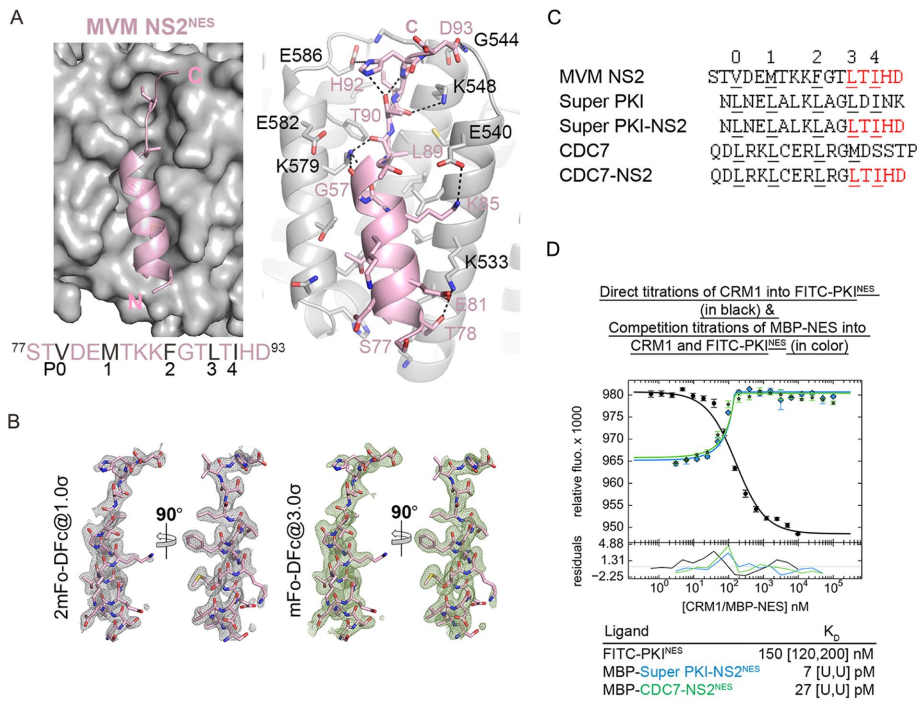
FIGURE 3: Crystal structure of MVM NS2^{NES} bound to CRM1 and design of picomolar affinity peptide inhibitors. (A) Left, MVM NS2^{NES} (pink cartoon) binds CRM1 (gray surface) like a typical class 1a NESs, with an N-terminal helix and C-terminal strand. Right, Details of CRM1-NES interaction. Black dotted lines show polar contacts within the NES (pink cartoon) and between the NES and CRM1 (gray cartoon). (B) Final refined model of the NES (pink sticks) overlaid onto electron density meshes of 2mFo-DFc map contoured at 1.0σ and kick OMIT map (calculated by omitting the NES peptide) contoured at 3.0σ. (C) Sequences of wild-type NES sequences and their chimera with MVM NS2^{NES}. Φ side chains in the NESs that bind hydrophobic pockets in the CRM1 groove are numbered and underlined. (D) Differential bleaching data of MBP-Super PKI-NS2^{NES} and MBP-CDC7-NS2^{NES} binding to CRM1. Direct titrations of FITC-PKI^{NES} to CRM1 and RanGTP are shown in black and competition titrations of MBP-NESs to FITC-PKI^{NES}, CRM1, and RanGTP are shown in color. Dissociation constants (K_d) are obtained from triplicate titrations and 95% confidence intervals are reported in brackets. U = cannot be defined.

that specifically and potently inhibits Kapβ2 (Cansizoglu et al., 2007). Finally, we also examined the effect of overexpression of Super PKI-NS2^{NES} on cytotoxicity to T-REx-293 cells using a tetracycline-induced expression system (Supplemental Figure S2B). Although overexpression of Super PKI-NS2^{NES} is cytotoxic, it does not alter the subcellular localization of endogenous CRM1 (Supplemental Figure S2C).

Conclusion

There is a strong correlation between CRM1-NES affinity and nuclear export activity for NESs that bind CRM1 with K_ds in the tens of nanomolar to tens of micromolar range. The wide affinity range for active NESs draws parallels with the Impα/NLS system, which was reported to have a range of affinity that spans at least two orders of magnitude (Hodel et al., 2006). Taken together, these wide ranges of binding affinities may correlate with CRM1 and Impα/β's ability to transport hundreds of cargo proteins with diverse signal sequences. However, once beyond K_d of 150 μM, NESs no longer seem to be exported into the cytoplasm. Conversely, when NESs have K_ds tighter than 5 nM, their nuclear export activities are significantly reduced. These extraordinarily tight-binding NES sequences are able to inhibit nuclear export of other NESs. On the basis of these findings, we designed two peptide inhibitors that bind CRM1 with subnanomolar affinity.

Cloning

NES sequences, along with three to five immediately adjacent residues on either ends, were cloned into different vectors used in this study (Table 2). To measure the in vivo activity and the in vitro binding affinity for CRM1, the same NES sequences were cloned into BamHI and XhoI sites of pEYFP$_2$-SV40^{NLS} and pMal-TEV vectors, respectively. For the use of peptide inhibition assay, MSM NS2^{NES}, Super PKI^{NES}, and Super PKI-NS2^{NES} were cloned into XhoI and HindIII sites of the pmKate2-C vector. All constructs were cloned using procedures as previously described (Xu et al., 2015) and verified by sequencing.

Quantitation of nuclear export activity

We developed a quantitation pipeline to measure the NES activity in live HeLa cells as illustrated in Figure 1A. The nuclear export activity of NESs was determined by measuring the steady-state distribution of fluorescence-tagged reporter proteins (EYFP$_2$-SV40^{NLS}-NES). HeLa cells were transiently transfected with different EYFP$_2$-SV40^{NLS}-NES constructs and live cell imaging was performed after 24 h. The ratio of cytoplasmic to nuclear YFP signal ($R_{C/N}$) was normalized by the corresponding $R_{C/N}$ after 5 nM leptomycin B (LMB) treatment of 16–18 h in duplicate wells. $R_{C/N}$ with LMB treatment can account for the passive export of reporter proteins by diffusion, as LMB specifically inhibits CRM1 export activity.

Live cell imaging was performed at 37°C in a 5% CO_2 atmosphere using a spinning disk confocal microscope system (Nikon-Andor) with a 40 × 0.6 NA air objective and the MetaMorph software. Z-stack images were obtained in the YFP and Hoechst channels using a step size of 0.6 μm (total z size 18 μm). In addition, a single differential interference contrast (DIC) image was taken in the middle of the z-stack. Cells were randomly selected for imaging if they 1) expressed YFP at adequate levels that the signal is not saturated, 2) contained no obvious abnormality observed under DIC, and 3) were not dividing, as evidenced by Hoechst staining.

The acquired z-stack images were imported into ImageJ (version: 1.49i) for further analysis. Four nuclear z-planes spanning the middle of the nucleus (total z size 1.8 μm) were selected and merged into a single YFP (by average intensity projection) and Hoechst image (by maximum intensity projection) for analysis. Watershed segmentation was applied to Hoechst images to define the nuclear region of interest (ROI). For each nuclear ROI, a cytoplasmic "ring" ROI with a thickness of 150 nm was generated by dilating the nuclear ROI twice and performing exclusive-or (XOR) operation on these two dilated areas in ImageJ. The mean intensities in nuclear and cytoplasmic ROIs were measured and exported to Microsoft Excel, where the ratio of cytoplasmic to nuclear YFP signal ($R_{C/N}$) was calculated.

Cell culture

HeLa cells from the American Type Culture Collection were cultured in DMEM (Sigma-Aldrich) supplemented with 10% fetal bovine

NES	Sequence	No. of cells	No. of experiments
PKI	[34]NSNELALKLAGLDINK[49]	108	12
CPEB4	[379]RTFDMHSLESSLIDIMR[395]	30	3
MEK1	[28]TNLEALQKKLEELELDE[44]	44	3
ADAR1	[121]RGVDCLSSHFQELSIYQ[137]	33	4
hRio2	[389]RSFEMTEFNQALEEIKG[405]	32	3
FMRP	[424]LKEVDQLRLERLQID[438]	37	3
Super PKI	[34]NLNELALKLAGLDINK[49]	32	3
X11L2	[55]SSLQELVQQFEALPGDLV[72]	59	3
NPM[mutA]	[278]MTDQEAIQDLCLAVEEVSLRK[298]	32	3
HIV Rev	[73]LQLPPLERLTLDC[85]	42	4
Pax	[264]RELDELMASLSDFKFMA[280]	37	3
mDia2	[1157]SVPEVEALLARLRAL[1171]	36	4
CPEB4-R	[395]RMIDILSSELSHMDFTR[379]	33	3
p73	[364]NFEILMKLKESLELMELVP[382]	48	4
HDAC5	[1081]EAETVSAMALLSVG[1095]	35	3
SMAD4	[134]ERVVSPGIDLSGLTLQ[149]	32	3
MVM NS2	[77]STVDEMTKKFGTLTIHD[93]	39	3
hRio2-R	[405]GKIEELAQNFETMEFSR[389]	33	3
HPV E7	[73]HVDIRTLEDLLMGTLGIVC[91]	40	3
CDC7	[456]QDLRKLCERLRGMDSSTP[473]	36	3
Stradα	[413]GIFGLVTNLEELEVD[427]	32	3
SNUPN	[1]MEELSQALASSFSVSQDLNS[20]	33	3
PKI (I47A)	[34]NSNELALKLAGLDANK[49]	46	7
PKI (L42A/L45A)	[34]NSNELALKAAGADINK[49]	45	5

TABLE 2: NES sequences, number of cells, and experiments in NES activity assay.

serum (FBS; Sigma-Aldrich) and 1% antibiotic-antimycotic (Life Technologies, Thermo Fisher Scientific) at 37°C in 5% CO_2.

Transfections
HeLa cells that were seeded onto glass-bottom 24-well culture plates (Phenix Research Products) and grown to 50–70% confluency. Transfections were performed according to the manufacturer's instructions with reduced DNA-to-reagent ratios of 1:1 (Lipofectamine 3000) or of 1:10 (Effectene), respectively. Cotransfection with red fluorescent protein (RFP)-NES was conducted using a transfection mixture of plasmid DNA at a reporter-to-inhibitor ratio of 1:9.

Quantitation of binding affinity for CRM1
The K_d values are obtained by competition differential bleaching experiments using a fluorescent probe FITC-PKI[NES] that bleaches at distinct rates when unbound and bound to CRM1. FITC-PKI[NES] undergo a reproducible differential bleaching when titrated with CRM1. The bleaching rate of the fluorescent probe is dependent on the concentration of the titrant CRM1, is saturable at high concentrations of CRM1, and can be fitted to a sigmoidal curve, which suggests a two-state behavior of the probe when it is unbound or bound to CRM1 (Fung *et al.*, 2015). Differential bleaching of the probe can be counteracted by titration of MBP-NESs. MBP-NESs compete with FITC-PKI[NES] for the NES-binding groove of CRM1 and the changes in bleaching rate of FITC-PKI[NES] will reflect the fraction of CRM1 bound to the FITC-PKI[NES] or to MBP-NES.

Therefore, different MBP-NESs can be titrated to compete with FITC-PKI[NES] for CRM1 to allow measurement of affinities of various MBP-NESs. Data were processed in PALMIST (Scheuermann *et al.*, 2016) using averages of triplicate experiments without weighted fitting. Confidence levels at 95% were obtained by error-surface projection method. Nine binding affinity data were measured in this study while the others were measured in our previous works (Fung *et al.*, 2015, 2017) and reanalyzed to obtain 95% confidence interval (see details in Supplemental Figure S3 and Table 1).

Statistical analysis
Mann–Whitney tests, *p* values (two-tailed), 95% confidence interval error bars, and Pearson correlation coefficients in this study were computed and calculated using the SciPy module of Python.

REFERENCES

Cansizoglu AE, Lee BJ, Zhang ZC, Fontoura BMA, Chook YM (2007). Structure-based design of a pathway-specific nuclear import inhibitor. Nat Struct Mol Biol 14, 452–454.

Conti E, Uy M, Leighton L, Blobel G, Kuriyan J (1998). Crystallographic analysis of the recognition of a nuclear localization signal by the nuclear import factor karyopherin α. Cell 94, 193–204.

Dong X, Biswas A, Chook YM (2009). Structural basis for assembly and disassembly of the CRM1 nuclear export complex. Nat Struct Mol Biol 16, 558–560.

Engelsma D, Valle N, Fish A, Salomé N, Almendral JM, Fornerod M (2008). A supraphysiological nuclear export signal is required for parvovirus nuclear export. Mol Biol Cell 19, 2544–2552.

Fanara P, Hodel MR, Corbett AH, Hodel AE (2000). Quantitative analysis of nuclear localization signal (NLS)-importin α interaction through fluorescence ddepolarization. J Biol Chem 275, 21218–21223.

Fornerod M, Ohno M, Yoshida M, Mattaj IW (1997). CRM1 is an export receptor for leucine-rich nuclear export signals. Cell 90, 1051–1060.

Fu S-C, Huang H-C, Horton P, Juan H-F (2012). ValidNESs: a database of validated leucine-rich nuclear export signals. Nucleic Acids Res 41, D338–D343.

Fukuda M, Asano S, Nakamura T, Adachi M, Yoshida M, Yanagida M, Nishida E (1997). CRM1 is responsible for intracellular transport mediated by the nuclear export signal. Nature 390, 308.

Fung HYJ, Fu S-C, Brautigam CA, Chook YM (2015). Structural determinants of nuclear export signal orientation in binding to exportin CRM1. Elife 4, e10034.

Fung HYJ, Fu S-C, Chook YM (2017). Nuclear export receptor CRM1 recognizes diverse conformations in nuclear export signals. Elife 6, e23961.

Güttler T, Madl T, Neumann P, Deichsel D, Corsini L, Monecke T, Ficner R, Sattler M, Görlich D (2010). NES consensus redefined by structures of PKI-type and Rev-type nuclear export signals bound to CRM1. Nat Struct Mol Biol 17, 1367–1376.

Hodel AE, Harreman MT, Pulliam KF, Harben ME, Holmes JS, Hodel MR, Berland KM, Corbett AH (2006). Nuclear localization signal receptor affinity correlates with in vivo localization in Saccharomyces cerevisiae. J Biol Chem 281, 23545–23556.

Hodel MR, Corbett AH, Hodel AE (2001). Dissection of a nuclear localization signal. J Biol Chem 276, 1317–1325.

Kırlı K, Karaca S, Dehne HJ, Samwer M, Pan KT, Lenz C, Urlaub H, Görlich D (2015). A deep proteomics perspective on CRM1-mediated nuclear export and nucleocytoplasmic partitioning. Elife 4, e11466.

Kobe B (1999). Autoinhibition by an internal nuclear localization signal revealed by the crystal structure of mammalian importin α. Nat Struct Mol Biol 6, 388–397.

Kosugi S, Hasebe M, Entani T, Takayama S, Tomita M, Yanagawa H (2008). Design of peptide inhibitors for the importin α/β nuclear import pathway by activity-based profiling. Chem Biol 15, 940–949.

Lott K, Bhardwaj A, Sims PJ, Cingolani G (2011). A minimal nuclear localization signal (NLS) in human phospholipid scramblase 4 that binds only the minor NLS-binding site of importin α1. J Biol Chem 286, 28160–28169.

Marfori M, Mynott A, Ellis JJ, Mehdi AM, Saunders NFW, Curmi PM, Forwood JK, Bodén M, Kobe B (2011). Molecular basis for specificity of nuclear import and prediction of nuclear localization. Biochim Biophys Acta 1813, 1562–1577.

Nakada R, Hirano H, Matsuura Y (2015). Structure of importin-α bound to a non-classical nuclear localization signal of the influenza A virus nucleoprotein., Structure of importin-α bound to a non-classical nuclear localization signal of the influenza A virus nucleoprotein. Sci Rep 5, 15055.

Ossareh-Nazari B, Bachelerie F, Dargemont C (1997). Evidence for a role of CRM1 in signal-mediated nuclear protein export. Science 278, 141–144.

Scheuermann TH, Padrick SB, Gardner KH, Brautigam CA (2016). On the acquisition and analysis of microscale thermophoresis data. Anal Biochem 496, 79–93.

Stade K, Ford CS, Guthrie C, Weis K (1997). Exportin 1 (Crm1p) is an essential nuclear export factor. Cell 90, 1041–1050.

Thakar K, Karaca S, Port SA, Urlaub H, Kehlenbach RH (2013). Identification of CRM1-dependent nuclear export cargos using quantitative mass spectrometry. Mol Cell Proteomics 12, 664–678.

Wen W, Meinkoth JL, Tsien RY, Taylor SS (1995). Identification of a signal for rapid export of proteins from the nucleus. Cell 82, 463–473.

Wu W, Sankhala RS, Florio TJ, Zhou L, Nguyen NLT, Lokareddy RK, Cingolani G, Panté N (2017). Synergy of two low-affinity NLSs determines the high avidity of influenza A virus nucleoprotein NP for human importin α isoforms. Sci Rep 7, 11381.

Xu D, Grishin NV, Chook YM (2012). NESdb: a database of NES-containing CRM1 cargoes. Mol Biol Cell 23, 3673–3676.

Xu D, Marquis K, Pei J, Fu S-C, Ca atay T, Grishin NV, Chook YM (2015). LocNES: a computational tool for locating classical NESs in CRM1 cargo proteins. Bioinformatics 31, 1357–1365.